Structural analysis and growing mechanisms for long SnO2 nanorods synthesized by spray pyrolysis

F. Paraguay-Delgado, W. Antúnez-Flores, M. Miki-Yoshida,

A. Aguilar-Elguezabal, P. Santiago, R. Díaz and J.A. Ascencio

Abstract

Flat-surfaced, rod-like materials were obtained by synthesizing long one-dimensional SnO2 structures using a new spray pyrolysis method. The structure and growing mechanisms were evaluated by using scanning and transmission electron microscopy and atomic force microscopy. Molecular simulation tools and high resolution transmission electron microscopy images allowed the analysis of a dynamic behaviour for energy release which determines how the structures are formed by searching for an axial energy release direction.

1. Introduction

Nanostructured materials have been widely used in many fields during the last few years, due to their interesting and unique properties, which arise due to the nanometric scale. In particular, one-dimensional nanostructures have attracted the attention of many researchers because of the possibility of applying them in near-future devices in sensors [1–3], catalysis [4–6], energy related devices [7–10], and many other devices. In addition, nanotubes, which are extensively studied hollowed structures [3, 4, 11], may have a cylindrical shape (an almost circular cross section view) [8–10, 12–14] or a flat, ribbon-like shape (a rectangular cross section view) with an aspect ratio >>1 [1, 2, 9, 15–17]. One-dimensional semiconductor structures have shown potential for applications in optoelectronic devices [18], gas sensors

[19], solar energy devices [10], and even for detecting leakages and reducing gases such as H2, H2S, CO, propane, and others [17]. SnO2 is one of the semiconducting oxides, that, together with ZnO, In2O3, and CdO, have unique properties and can be used as transparent conducting materials [20] and gas sensors [21]. In particular, SnO2 has acquired significant importance because of its high capacity for evaluating low concentrations of flammable gases [21]. In the first report of a SnO2 nanobelt, by Wang et al [1], it was obtained by a thermal evaporation method, opening a wide scope for synthesis methods to produce large-scale nanobelts [22] and corresponding studies concerning the structure [23] and growing modes of the new forms produced [24], and even for the production of ordered SnO2 nanowire arrays [25]. Recently, several researchers synthesized ultralong, beltlike, rutile SnO2 structure by metal oxide powder thermal evaporation [16, 23] or elemental tin fast oxidation [26]. Both syntheses require very high temperature (>1000 ◦C). Besides this, the production of single-crystalline materials, based on the vapour–liquid–solid (VLS) process for nanorod growth by a catalysis-assisted method [27], requires small metal clusters at the growing extreme of the nanorod. Another way of achieving growth is based on using vapour–solid mechanisms at high temperature to generate a continuous SnO2 deposition [23, 28]. An interesting analysis is shown by Ma et al [24], who proposed a SnO decomposition process that results in SnO2 nuclei cluster precipitation for the growing nanobelts. This process suggests that the temperature changes the rod growth along an axis, which allows internal process energy to arise. A layer-by-layer mode of growth for producing longer structures is also mentioned, based on a zigzag surface, but an influence of temperature on the

nanobelt blended forms is also proposed. In the present study, the synthesis of bulk quantities of SnO2 nanorods by a simple spray pyrolysis method is reported; this represents an important improvement because considerable quantities can be continuously produced. This report is focused on structural nanorod analysis, and strong evidence to support a suggested growth mechanism—with the help of two-dimensional images from scanning electron microscopy (SEM) and high resolution transmission electron microscopy (HRTEM)—is found. A three-dimensional (3D) analysis by means of scanning probe microscopy (SPM) is presented, which gives important evidence of boundary effects impossible to obtain with the HRTEM and it also allowed us to study the early stages of nanorod production on the substrate surface.

2. Experimental methods

Tin oxide nanorods were grown inside Vycor tubing using the spray pyrolysis method; their dimensions were: internal diameter of 7 mm and length of 500 mm. The tubing was connected to a pneumatic nebulizer, which was used as an atomizer. The airflow was regulated with a mass flow controller. The tubing was heated at around 900 ◦C in a horizontal Lindberg Scientific furnace. The starting solution was 0.05 M of tin tetrachloride (Aldrich) diluted in methanol. Synthesis by spray pyrolysis involves the atomization of a precursor solution into very small discrete droplets. These droplets are subsequently transported through the tube, where the solvent evaporates and the dissolved species react to form the product. The nanorods were obtained on the tubing surface, mostly in a radial direction, i.e. perpendicular to the glass. The samples were collected by simple scratching or by

means of an ultrasonic acetone bath; then they were deposited onto a sample holder for the SEM and SPM analysis, while a drop of the material dispersed in acetone was placed on a copper grid, to be analysed using the HRTEM. SEM micrographs were obtained from a JSM-5800LV scanning electron microscope, together with a DX-4 x-ray energy dispersive spectrometer (EDS), for evaluating the surface morphology, working at 15 keV. For HRTEM images, CM200 and JEM 2010F microscopes with an EDS were used for elemental analysis. Finally, a Nanoscope IV SPM from Digital Instruments, by Veeco, was used in tapping mode to evaluate the sample's height and phase. On the basis of SnO2 crystal parameters and using the Cerius software from Accelrys [29], a superlattice model was built by following the observed experimental growth conditions. Minimal energy optimization was obtained using

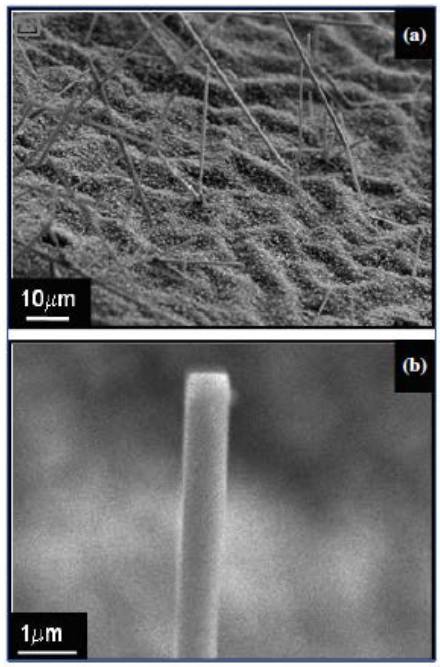

Figure 1. Scanning electron microscopy images from the SnO_2 production: (a) 500× (showing the inside surface of the tube) and
(b) 10 000× (where the details of the top of a SnO_2 nanorod, grown on the glass surface can be seen) micrographs.

a force field parameterized by means of density functional theory (DFT) calculations [30]. The analytical data allowed the building of models equivalent to the structures that were experimentally observed. HREM images were obtained with the Simula TEM program developed by Gomez et al [31] which is based on the multislice method.

3. Results and discussion

Samples deposited under optimum conditions produced a filmlike structure inside the tubing, composed of long structures and small nanorod-like morphologies. SEM micrographs for selected samples are shown in figure 1. In figure 1(a), long rods and small material fragments can be identified on the substrate; the longest rods were around 200 µm long. At higher magnification, it can be observed that the rods have flat surfaces, similar to the small aggregates adhering to the substrate; however, when the structures grow they tend to have ribbon-like morphologies. In figure 1(b), the structure tip has rectangular, flat-end profiles, and a thickness of 800 nm. This low magnification analysis matches with previous SnO2 nanorod reports. Also, TEM analysis showed a high similarity of our nanorods with materials reported by several groups [1, 6–8]. In figure 2, a local study of the onedimensional structure is presented, showing a long, very thin nanostructure. Figure 2(a) shows a general view of a long nanorod, with a length of more than 4 µm, and a width of around 150 nm. Figure 2(b) shows the selected area ‘1’ marked in figure 2(a); demonstrating the local contrast of internal

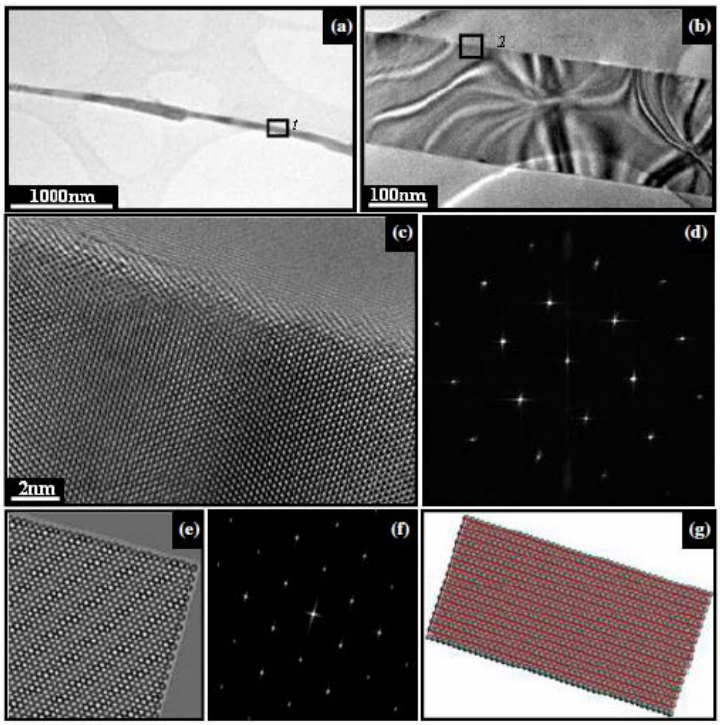

Figure 2. TEM images of (a) a long ribbon-like form with (b) a magnified selected area (1) and (c) a second enlargement from the marked selected area (2) to show the high resolution contrast and (d) the corresponding FFT. The simulated (e) HREM image and (f) FFT with (g) the atomic model considered are also shown for clarity.

fringes which are usually straining the material. A selected area '2' from the previous image is observed (figure 2(c)); the high resolution image allows the measurement of interplanar distances of 3.65 and 2.37 Å that correspond to (110) and (200) SnO2 planes, respectively. In fact, the lattice resolution shows no defect evidence, which is similar to the reported results of other works [16, 23]. The corresponding fast Fourier transformation is shown in figure 2(d). In order to achieve a better understanding of the structure, a simulated HREM image under the same experimental conditions is shown (figure 2(e)); this image is similar to figure 2(c). Image 2(f) is fast Fourier transform (FFT) of figure 2(e) and it is similar to the one shown in figure 2(d). The model used for the HRTEM image is shown in figure 2(g); it is a SnO2 super lattice growing in the [001] direction and observed in {010}

orientation. The structures are basically homogeneous and they are growing preferentially as one-dimensional crystal. However, it is well understood that TEM images correspond to twodimensional projections from three-dimensional samples and the information about the third dimension of these materials is lost. In order to resolve the third dimension, a SPM analysis in a tapping mode was realized, which permitted us to get information on thicker rods and to reproduce 3D details. Using the SPM, 50 nm to several µm wide nanorods were found. Figure 3(a) shows a selected area (10 µm × 10 µm scan), where two rods of different size and shape can be identified. The largest belt belongs to a 58µm length structure, with almost flat surfaces, while the smallest one has a length of 12 µm and an irregular surface with multiple faces parallel to the growing axis. This was done by using the transverse section analysis in figures 3(b) and (c) respectively, for each belt in the selected areas ‘B’ and ‘C’ shown in figure 3(a). Figure 3(b) shows the corresponding biggest wire profile, which has a trapezoidal shape with a maximum height of 2.47 µm, while its width is reduced from 2.94 µm in the basis to 1.85 µm. Figure 3(c) shows the corresponding smallest rod profile, which has a high roughness, a maximum height of 1.03 µm, and a basis width of 1.98 µm showing multiple faces. In order to achieve a better understanding of the observed rods, an atomistic model for each profile analysed is included. Figure 3(d) clearly shows how the top of the rod is determined by the flat faces, and surface changes correspond to extra layers. Besides this, figure 3(e) shows how the formation of flat surfaces produces a different slope and roughness. In fact, this analysis allows the understanding of different kind of surface formation; however, these structural characteristics are not observed with a

perpendicular electron beam. Besides this, searches for zones of the sample where the nanorods are not large can be carried out, and how the material forms during the earliest stages of nanorod formation can be studied; this is done by means of SMP micrographs as shown in figure 4, which presents a 3D image of the early formed

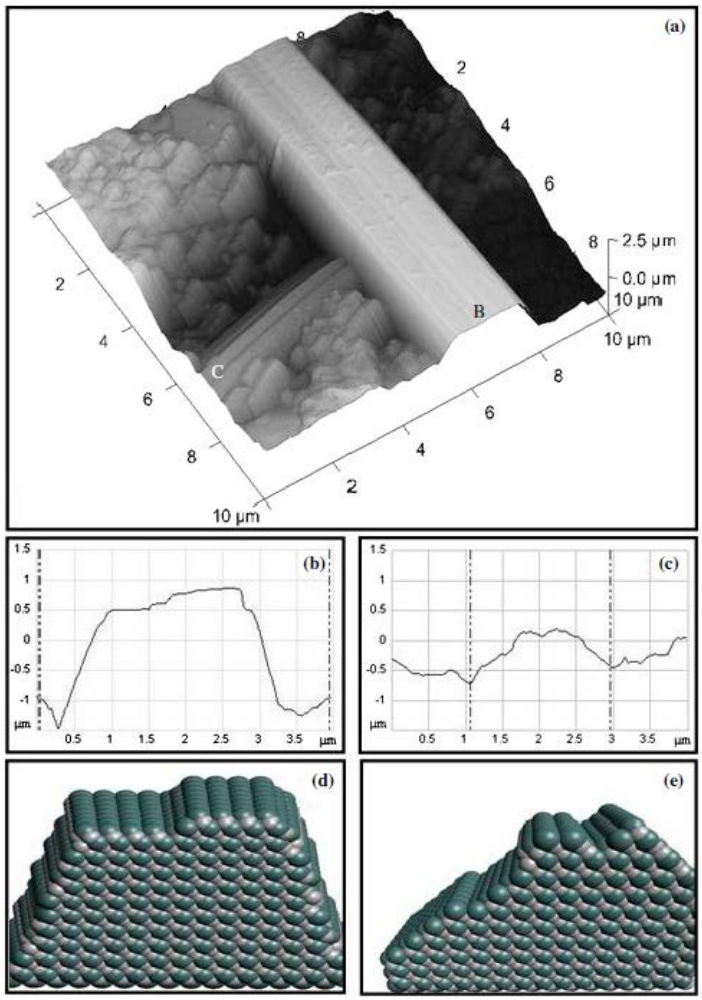

Figure 3. (a) A SPM 3D image for a couple of nanorods with their corresponding section analysis to allow study of their profiles ((b) and (c)) and their 3D image, for the early stages of the growing process ((d) and (e)).

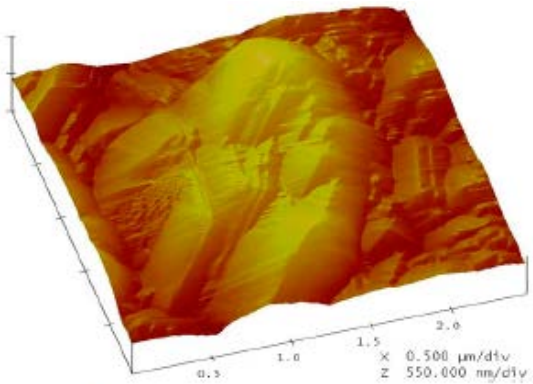

Figure 4. An 3D image for the early stages of the growing process obtained with the tapping mode of the SPM.

crystals producing a multiple layer structure and square angle morphology. These shapes denote a preferential [001] growing axis, which is similar to the one observed for the previous nanorods [1]. The 3D information observed with the SPM allows the identification of layers in the growing process of the one-dimensional structures; however, this evidence, which was carefully searched for, must be confirmed by atomistic resolution, as it is observed in small regions of the samples. This evidence is shown in figure 5, and it is mainly identified as small lattice deformations; it requires careful observation to notice them in the image (figures 5(a) and (b)). The corresponding fast Fourier transform is included in each image. Using these images makes it possible to determine a hexagonal array, but also in the corresponding FFT for figure 5(a) dots longer than the ones in figure 5(b) can be seen, which is extra evidence for small lattice deformation. Besides this, the presence of two tin oxide phases is distinguished in a few regions of the samples, as shown in figures 5(c) and (d), where

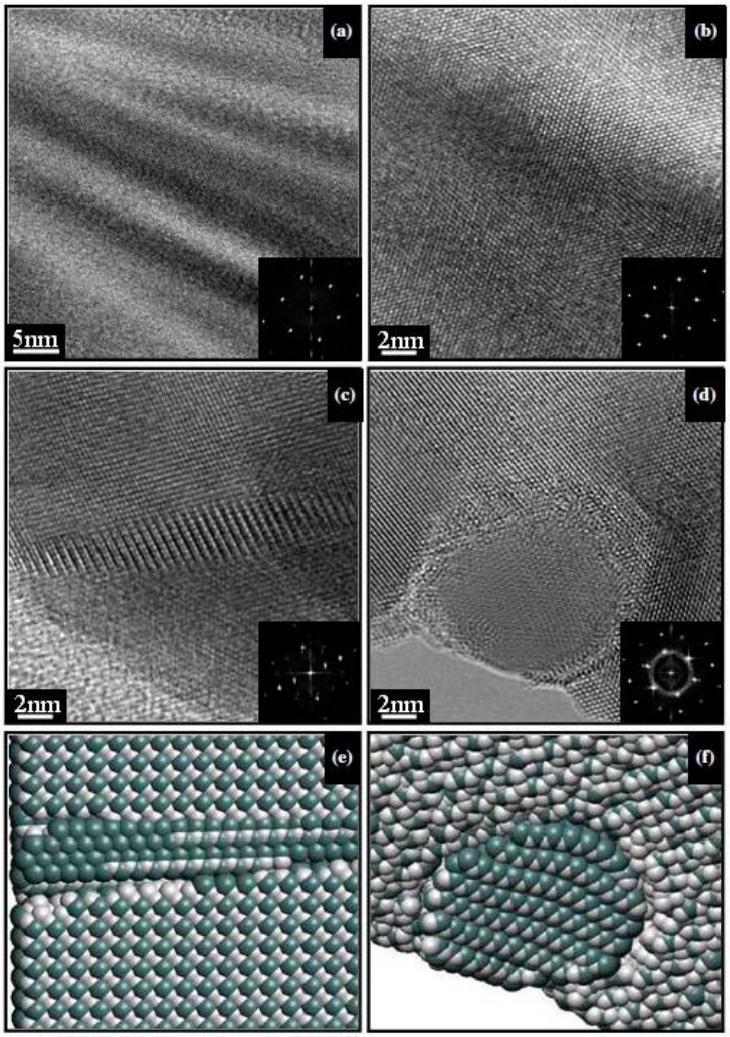

Figure 5. HRTEM images of defects in one-dimensional structures. The fringe contrast of this image shows small strain effects in the material ((a) and (b)), while atomic resolution clearly shows this strain effect in the crystalline SnO_2 structure. Another defect that can be observed is the presence of small regions of SnO, both as a layer (c) and as clusters on the material's borders (d). These effects are supported by the models shown in (e) and (f).

SnO inclusions are identified as small layers (5(c)) and small clusters (5(d)) inside the SnO2 crystalline matrix; this effect can be noticed because of the differences of the lattice spacing of both zones in relation to the SnO2 matrix. In fact, the use of models allows a better understanding, as observed in figures 5(e) and (f). The models correspond to lower energy structures obtained after a geometry optimization using the parameterized force field method. This evidence just implies local deformation, and layerby layer formation must be better supported. So then an

electron beam was used in a small region of the nanorod thin boundaries, where layer effects can be distinguished in the rod's corner. Dynamic changes can take place on applying the electron beam, as was demonstrated before [32–34]; such changes can be observed in the structure shape and HREM contrast, which is associated with a process of reconstructing atomistic distribution in a wave-like behaviour. In the sequence of figure 6, four steps of this process can be observed, which show evidence of layer-by-layer nanorod formation. The sequence is produced with an electron beam which requires low energy, in contrast with the formation temperatures. However, small changes are observed in the stacking faults marked with the dotted arrow, where also atomic reordering is observed on the surface. In the regions marked with the solid arrow, an atomic reconstruction is observed, reaching flat faces and apparently reducing nanorod strain. Finally, the area closest

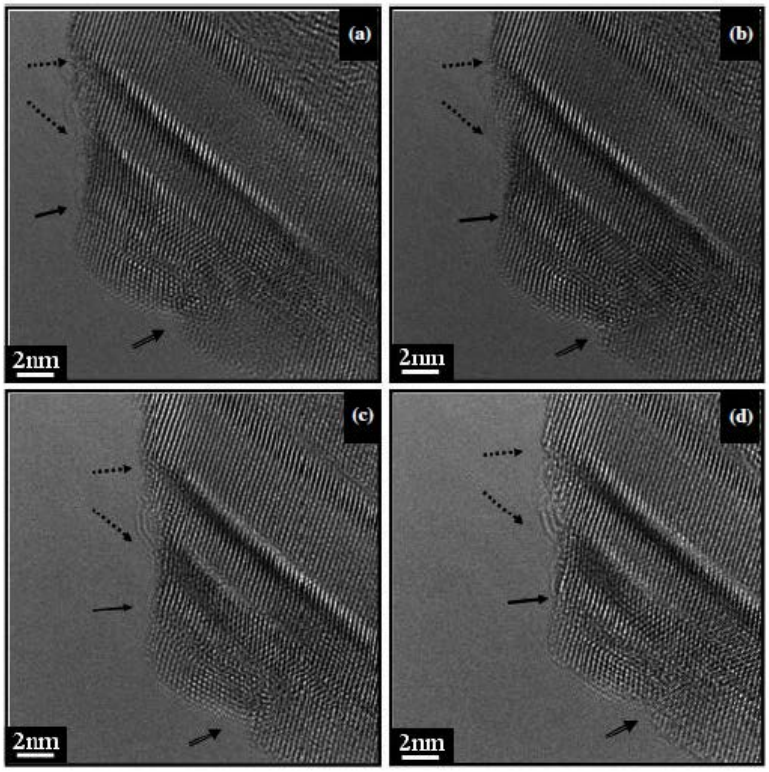

Figure 6. HREM images of an *in situ* analysis of the energy release process induced by the electron beam.

to the tip, marked with the double arrow, shows how energy release must produce flat tips when the layers are totally reorganized and aligned. Structural changes on the nanorod border involve a physical–chemical process of energy release from the internal atomic distribution to the boundaries, which is also related to the fringes commonly observed at lower magnifications (as shown in figure 2). This energy release process is, without doubt, motivated by the temperature in the formation process, but in HRTEM observations, the electron beam's own energy induced by the electron beam helps to distinguish changes in the material.

4. Conclusion

Long nanorods can be produced at low temperatures by the spray pyrolysis method. We have obtained one dimensional, flat-surfaced structures with large

crystalline domains However, 3D analysis has shown that these materials are not completely flat and the main evidence showed a layerby-layer growth construction process. The structures are not totally flawless, but most of the material shows a crystalline periodicity. The presence of linear defects and local layer arrays was demonstrated. This layerby-layer process is directly related to the initial stages that are analysed and determined as being formed by rectangular, parallel growing domains which form long structures, where strain energy is high and there is a continuous energy release process that produces the single-crystal domain. Our knowledge about growing mechanisms involved in nanorod formation was greatly increased by this research, and it also offers the possibility of manipulating the surface to produce hot points for catalysis applications and also for producing changes in nanorod direction by means of sudden temperature changes used to produce one-dimensional nanostructures.

Acknowledgments

The authors wish to thank Dr G Canizal for his valuable help in SPM studies, Mr L Rendon for his technical support in obtaining HREM images, and D Lardizabal, E Torres and I Estrada for technical support. We also wish to thank CUDI Mexico for partially supporting the UNAM-IMP project named ‘Study and structural characterization of one-dimension systems using JEM-2010F FasTEM microscopy by remote control using Internet2’. Finally, we wish to thank Conacyt 34310-U for supporting this project.

References

[1] Pan Z W, Dai Z R and Wang Z L 2001 Science 291 1947

[2] Kong J, Franklin N R, Zhou Ch, Chapline M G, Peng S, ChoK and Dai H 2000 Science 287 622

[3] Ghosh Sh, Sood A K and Kumar N 2003 Science 299 1042

[4] Parrilla P A, Dollon A C, Jones K M, Reiker G, Schulz D L, Ginley D S and Heben M J 1999 Nature 397 114

[5] Fukuoka A, Araki H, Sakamoto Y, Inagaki S, Fukushima Y and Ichikawa Y M 2003 Inorg. Chim. Acta 350 371

[6] Liu Z Q, Pan Z W, Sun L F, Tang D S, Zhou W Y, Wang G, Qian L X and Xie S S 2000 J. Phys. Chem. Solids 61 1171

[7] Huynh W U, Dittmer J J and Alivisatos A P 2002 Science 295 2425

[8] Shen G, Chen D, Tang K, Qian Y and Zhang S 2003 Chem. Phys. Lett. 375 177

[9] Wang Z, Shimizu Y, Sasaki T, Kawaguchi K, Kimura K and Koshizaki N 2003 Chem. Phys. Lett. 263 663

[10] Han K R, Kim Ch S, Kang K T, Koo H J, Kang D L and Jingwen H 2002 Sensors Actuators B 81 182

[11] Iijima S 1991 Nature 354 56

[12] José -Yacamán M, Ascencio J A and Canizal G 2001 Surf. Sci. Lett. 486 L449

[13] Ascencio J A, Santiago P, Rendon L and Pal U 2004 Appl. Phys. A 78

5

[14] Canizal G, Ascencio J A, Gardea-Torresday J and José -Yacaman M 2001 J. Nanop. Res. 3 475

[15] Arnold M S, Avouris P, Pan Z W and Wang Z L 2003 J. Phys. Chem. B 107 659

[16] Dai Z R, Gole J L, Stout J D and Wang Z L 2002 J. Phys. Chem. B 106 1274

[17] Santos J P and Agapito J A 1999 Thin Solid Films 338 276

[18] Ding J, McAvoy T J, Cavicchi R E and Semacik S 2001 Sensors Actuators B 77 597

[19] Korotcenkov G, Brinzari V, Schwank J, DiBatista M and Vasiliev A 2001 Sensors Actuators B 77 244

[20] Ginley D S and Bright C 2000 Mater. Res. Soc. Bull. 25 15

[21] Yamazoe N 1991 Sensors Actuators B 5 7

[22] Sun S H, Meng G W, Wang Y W, Gao T, Zhang M G, Tian Y T, Peng X S and Zhang L D 2003 Appl. Phys. A 76

[23] Zhang J, Jiang F and Zhang L 2003 J. Phys. D: Appl. Phys. 36 L21

[24] Ma X L, Li Y and Zhu Y L 2003 Chem. Phys. Lett. 376 794

[25] Zheng M J, Li G H, Zhang X Y, Huang S Y, Lei Y and Zhang L D 2001 Chem. Mater. 13 3859

[26] Maiti A, Rodriguez J A, Matthew L, Kung P, KcKinney J R and Yang P 2003 Nano Lett. 3 1025

[27] Duang X F and Leiber C M 2000 Adv. Mater. 12 298

[28] Yang P and Lieber C M 1997 J. Mater. Res. 12 2981

[29] Cerius[2]Software 2000 Accelrys. San Diego, CA

[30] Khon W and Sham L 1965 J. Phys. Rev. 140 A1133

[31] Gomez-L A, del Rio Beltran and SimulaTEM

software http://fisica.unam.mx

[32] Ascencio J A, P´erez M, Tehuacanero S and

Jos´e-Yacam´an M 2001 Appl. Phys. A 73 295

[33] Ascencio J A, Mendoza M, Santamar´ıa T, P´erez M, Nava I, Guti´errez-Wing C and Jos´e-Yacam´an M 2002 J. Cluster Sci. 13 189

[34] Jos´e-Yacam´an M, Ascencio J A and Canizal G 2001 Surf. Sci. Lett. 486 L449